

**'Artificial atoms' in magnetic fields:
Wave function shaping and phase sensitive tunneling**

Wen Lei,^{1,2} Christian Notthoff,¹ Jie Peng,³ Dirk Reuter,⁴

Andreas Wieck,⁴ Gabriel Bester,³ and Axel Lorke^{1,*}

¹*Department of Physics and CeNIDE, University of Duisburg-Essen,
Lotharstr. 1, 47048 Duisburg, Germany*

²*Department of Electronic Materials Engineering,
RSPE, Australian National University,
Acton, Canberra ACT 0200, Australia*

³*Max-Planck-Institut für Festkörperforschung,
Heisenbergstr. 1, 70569 Stuttgart, Germany*

⁴*Lehrstuhl für Angewandte Festkörperphysik, Ruhr-Universität Bochum,
Universitätstr. 150, 44780 Bochum, Germany*

(Dated: July 13, 2010)

*Electronic address: axel.lorke@uni-due.de

Symmetries are among the most fundamental concepts in physics. They determine basic conservation laws as well as the specific properties of everyday objects as exemplified in solid state physics by the vastly different properties of graphite and diamond, which only differ in their crystalline atomic arrangement. Systems which have different – sometimes conflicting– symmetries, are of particular interest, since they may exhibit intriguing properties; one of the best examples being the self-similar energy structure of a crystal in high magnetic fields, known as the Hofstadter Butterfly[1]. In this case the periodic translationally invariant square lattice is in conflict with the rotational magnetic field and leads to a fractal energy manifold. A simple system, which features multiple symmetries, is a charged particle, confined in a two-dimensional harmonic oscillator potential – a textbook problem in quantum mechanics, which is separable in either cartesian or cylindrical coordinates. The corresponding rectangular or circular symmetries can be lifted selectively by the application of a magnetic field or by an elongation of the confining potential, respectively. A competition arises when both perturbations are present, and, depending on their relative strength, the character of the eigenstates will tend towards circular or rectangular symmetry. The application of a magnetic field will also impose a sense of rotation upon the system, which can be expressed as the sign of the phase θ in the azimuthal part of the wave function, $e^{\pm i|\theta|}$.

It is the purpose of this communication to demonstrate how the concept of competing symmetries can be investigated in fully quantized few electron systems, using wave function mapping, and how the wave functions can be altered from rectangular symmetry towards circular symmetry by the application of a magnetic field. Furthermore, we will show that under suitable conditions, the tunneling maps are not only sensitive to the shape –or more precisely the amplitude– of the wave functions but also to their relative phase.

The system under investigation is an ensemble of self-assembled InAs quantum dots, grown on GaAs using the now well-established Stranski-Krastanov growth mode [2]. These dots can be charged by single electrons and holes and exhibit a variety of phenomena known from atomic physics, such as a shell structure [3–5], direct and exchange Coulomb interaction [6], spin multiplet formation and incomplete shell filling [7]. They are thus often referred to as 'artificial atoms'. Previous studies have shown that the properties of electrons, confined

in self-assembled quantum dots, can be well described using a two-dimensional parabolic harmonic oscillator potential [6]. For the present study, the dots are embedded in a field-effect transistor structure, shown schematically in Fig. 1, left. When a voltage V_g is applied to the top electrode (gate), the potential energy of the dots is shifted with respect to the back electrode. Thus, with increasing voltage, more and more electrons will be transferred from the back contact into the dots by tunneling through the barrier separating back contact and dots. Up to 6 electrons can be loaded into the dots, and the gate voltage for each tunneling event can be determined by simultaneously monitoring the capacitance of the sample (see Fig. 1, right). More details on the capacitance spectroscopy and the structure of the investigated samples can be found in Refs. [3, 4, 8, 9] and in section 'Methods', below.

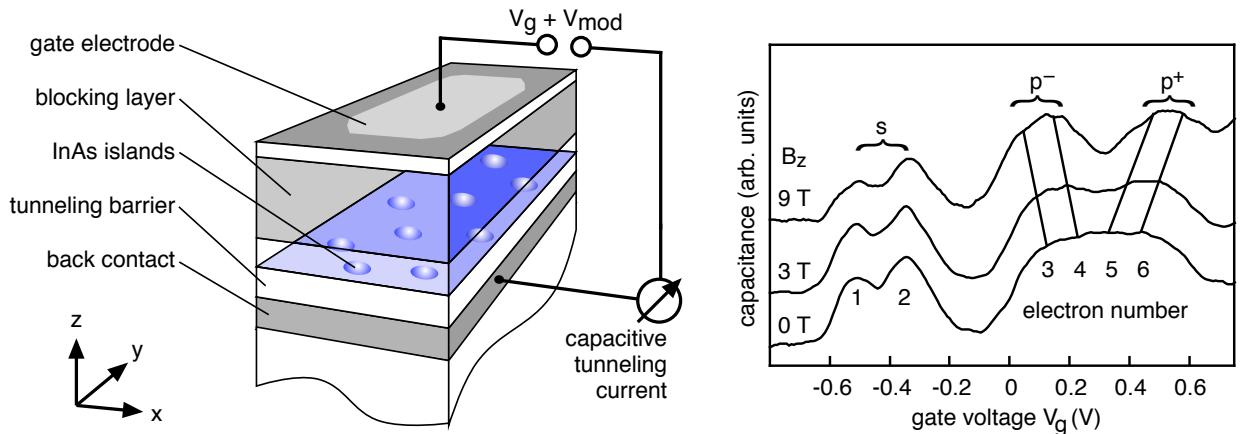


FIG. 1: Left: Schematic sample structure. The InAs quantum dots are embedded in a GaAs/(AlGa)As heterostructure and supplied with electrons from the highly doped back contact through the GaAs tunneling barrier. The number of electrons per dot can be tuned by the gate voltage and monitored by capacitance spectroscopy. Right: Capacitance-voltage traces, showing the subsequent filling of the InAs islands with 1 to 6 electrons. The first two electrons form the so-called 's-shell', the 3rd to 6th electron the 'p-shell'. With increasing magnetic field B_z , the p-shell exhibits Zeeman splitting with two states decreasing in energy (p^-) and two increasing (p^+).

To map out the wave function, we use a magneto-tunneling technique, developed by Patanè *et al.* [5, 10] and adapted to capacitance spectroscopy by Wibbelhoff *et al.* [8]: For sufficiently high AC frequencies, the capacitance signal is determined by the tunneling probability, which in turn is given by the overlap of the wave functions in the back contact and the dot [11]. Furthermore, as a consequence of the Lorentz force, an electron that

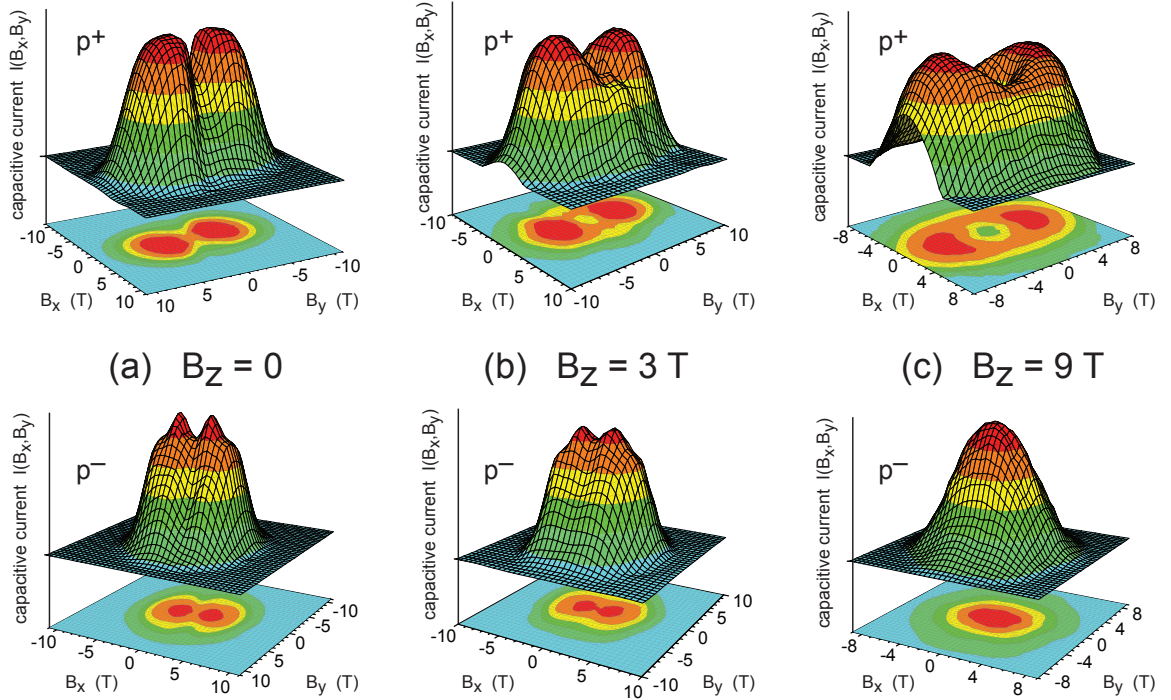


FIG. 2: Experimental maps of the tunneling current (capacitance amplitude) between the back contact and the dot layer as a function of the in-plane magnetic field (B_x, B_y) for different constant perpendicular fields B_z . With increasing B_z , the maps develop from a x - y -symmetry towards circular symmetry.

tunnels a distance Δz will experience a shift in momentum k_y , when a magnetic field B_x is applied,

$$\Delta k_y = \frac{eB_x}{\hbar} \Delta z. \quad (1)$$

Therefore, by recording the capacitance amplitude as a function of the in-plane magnetic field $I(B_x, B_y)$, a map of the probability density in momentum space $|\Psi(k_x, k_y)|^2$ can be obtained [5, 8, 10, 12]. Figure 2(a) shows such maps, obtained for the so-called "p-shell" of the quantum dots. This shell comprises two orbital states. One, labelled p^- , with a node along the x -axis (given by the $[1\bar{1}0]$ -direction of the GaAs crystal) and the other (p^+) with a node along the y -axis ($[110]$ crystal direction) [8, 13]. Because of anisotropic epitaxial growth

and strain [14], the p^- -state is somewhat lower in energy than the p^+ -state, which gives the wave functions the distinct x - y -symmetry, seen in Fig. 2(a). This can be accounted for by a slight elongation of the parabolic model potential $V(x, y) = \frac{1}{2}m\omega_0^2((1 + \Delta)x^2 + (1 - \Delta)y^2)$, where m is the effective mass, ω_0 the characteristic frequency of the parabolic confinement, and Δ a parameter, which determines its ellipticity.

Figures 2(b) and (c) demonstrate the influence of an additional magnetic field component B_z (perpendicular to the plane of the dots) on the capacitive current $I(B_x, B_y)$. It can clearly be observed that the magneto-tunneling maps exhibit more and more circularly symmetric character as the perpendicular magnetic field is increased. In the most simple approach, this can be attributed to a mixing of the x - and y -oriented states, caused by the Lorentz force. In particular, the map of the p^+ state develops towards the ring-like shape expected for orbitals with non-vanishing angular momentum in high magnetic fields. This shows how the competition between the anisotropic confinement potential and the magnetic forces determines the character of the wave function and how the external magnetic field can be used as an *in-situ* tuning parameter to shape the wave function from pure rectangular symmetry (Fig. 2(a)) towards a more circular structure (Fig. 2(c)).

As seen in the lower row of Fig. 2, also the p^- -maps exhibit a pronounced magnetic field dependence, however, they do not develop a ring-like shape. This is surprising at first, because in high magnetic fields, the wave functions of both p -states should exhibit a clear minimum in the center (see below). It should be kept in mind, though, that a direct relationship between the tunneling map $I(B_x, B_y)$ and the probability density in momentum space, $|\Psi(k_x, k_y)|^2$, is only given for vanishing perpendicular field, $B_z = 0$, as in Fig. 2 (a). Therefore, a more in-depth treatment of the magneto-tunneling with arbitrary field orientation is necessary in order to properly interpret the tunneling maps.

Our model is an extension of the approach of Patanè *et al.* [10] and takes into account the influence of B_z on the states in both emitter and dot. For simplicity, we assume the emitter to be two-dimensional [15] and take the text-book result for its wave functions in symmetric gauge, using cylindrical coordinates (r, θ) [16]:

$$\phi_{nl}^E(r, \theta) = e^{il\theta} \exp\left(-\frac{r^2}{4l_B^2}\right) r^{|l|} \mathcal{L}_{n-1}^{|l|}\left(\frac{r^2}{2l_B^2}\right). \quad (2)$$

Here, n and l are the radial and azimuthal quantum numbers, respectively, $l_B = \sqrt{\hbar/|eB_z|}$

is the magnetic length, and \mathcal{L} is the associated Laguerre polynomial. As in the treatment of the 3-dimensional back contact [10], we assume that tunneling is dominated by the state with the lowest in-plane energy, which, here, is the lowest Landau level with $n = 1$ and $l \leq 0$ [16]. This energy level is highly degenerate with respect to (negative) l . The probability density of the states with $l = 0, -1, -2$ are plotted for magnetic fields $B_z = 1, 3,$ and 9 T in the top of each panel in Fig. 3.

To obtain the wave functions of an elliptical quantum dot in a magnetic field, we utilize a finite element method, based on a triangular grid and a linear basis function set. The eigensolver employs the conjugated gradient minimization of the Rayleigh-quotient and a Ritz-projection to obtain few eigenvalues and vectors simultaneously. The characteristic frequency, the effective mass, and the anisotropy parameter are chosen to be $\hbar\omega_0 = 60$ meV, $\Delta = 0.1$, and $m = 0.07m_0$, respectively. The leftmost column in Fig. 3 shows the calculated dot wave functions for magnetic fields $B_z = 1, 3,$ and 9 T. As mentioned above, *both* p -states develop from rectangular towards circular symmetry with a distinctive minimum in the center.

Starting from Bardeen's tunneling theory, it can be shown that the measured tunneling current I is to a good approximation given by the overlap of the wave functions in the back contact and the dot [10, 11]. For the present case, which involves degenerate emitter states $l = 0, -1, -2, \dots$ we find:

$$I \propto \sum_{l \leq 0} \left| \int \psi^{\text{QD}*}(\mathbf{r}) \phi_{0l}^{\text{E}}(\mathbf{r}) d\mathbf{r} \right|^2. \quad (3)$$

The shift in momentum caused by the in-plane field (see Eq. 1) is taken into account by Fourier transformation $\psi^{\text{QD}}(\mathbf{r}), \phi^{\text{E}}(\mathbf{r}) \xrightarrow{FT} \psi^{\text{QD}}(\mathbf{k}), \phi^{\text{E}}(\mathbf{k})$ and addition of a momentum contribution $\hbar(\Delta k_x, \Delta k_y) = (B_y, B_x)\Delta z$, which finally leads to the relation between the signal $I(B_x, B_y)$ and the considered wave functions

$$I(B_x, B_y) \propto \sum_l \left| \iint \psi^{\text{QD}*}(k_x, k_y) \phi_{0l}^{\text{E}}(k_x - \Delta k_x, k_y - \Delta k_y) dk_x dk_y \right|^2. \quad (4)$$

In Fig. 3 the different contributions to the sum are shown in table form for the first three quantum dot states (s, p^-, p^+) and three Landau states ($l = 0, -1, -2$). The color scales are normalized between 0 and a maximum value, which is given in the bottom left of each plot. From these numbers, it can be seen that the contribution to $I(B_x, B_y)$ rapidly

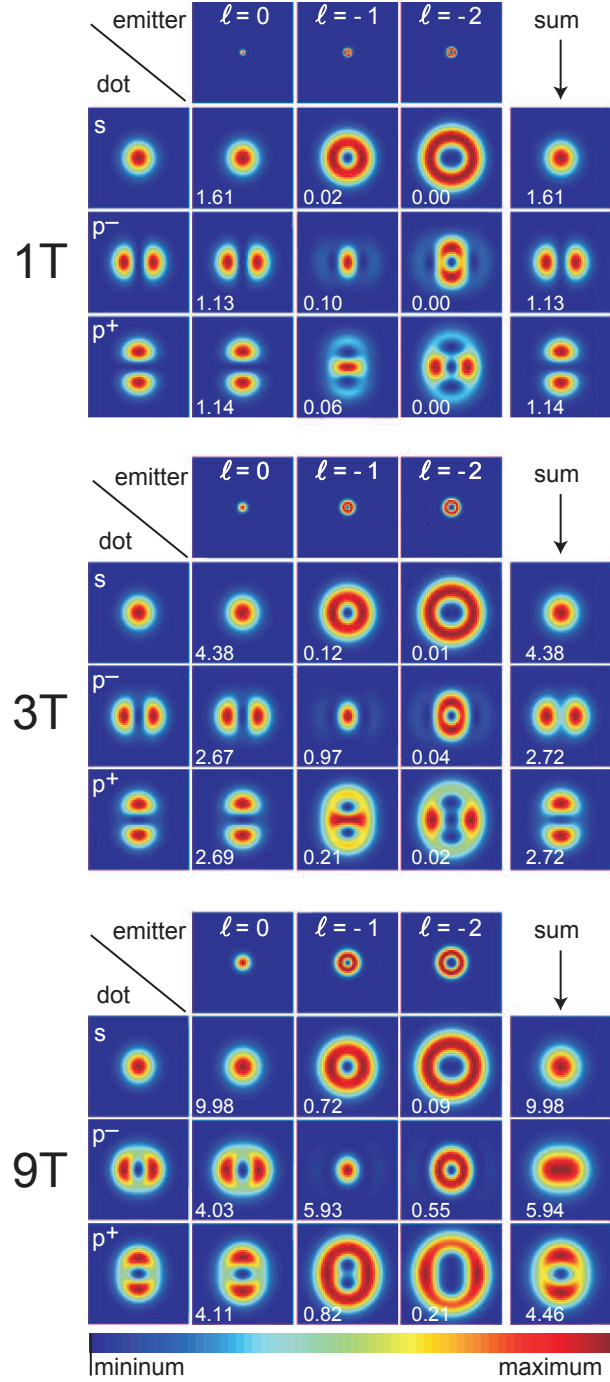


FIG. 3: Calculated momentum space representation of the lowest quantum dot states (s , p^+ and p^- , leftmost column) and three degenerate emitter states of the lowest Landau level (angular momentum $l = 0, -1, -2$, top row). The center panels show the overlap integrals of these states in matrix form. The number in each panel indicates the maximum of the color scale. The rightmost column depicts the sum of the overlap integrals, which corresponds to the calculated magnetotunneling signal. The plots scan a range of $\pm 8 \times 10^8 \text{ m}^{-1}$, which corresponds to a field of -13 to 13 Tesla.

decreases with increasing $|l|$. This is because with increasing angular momentum, the radius of the cyclotron orbit increases, which reduces the spatial overlap with the dot states and justifies the restriction to $l = 0, -1, -2$. The rightmost column shows the sum of the different contributions, which can be directly compared with the calculated probability density (leftmost column) and the experimental results. For the higher lying p^+ -state, we find that indeed, the magneto-tunneling amplitude gives an accurate representation of the original wave function. Furthermore, we find good qualitative agreement between the calculation and the corresponding magneto-tunneling maps shown in Fig. 2, top. For the lower p^- -state, we also find that the experimental data (Fig. 2, bottom), is well reproduced by the calculated sum. In this case, however, the magneto-tunneling maps do not match the shape of the wave function in the dot. In fact, not even the central node of this wave function is preserved and instead, the map exhibits a single maximum at the origin.

The leftmost column in Fig. 3 shows that – apart from a rotation by $\pi/2$ – the p^- and p^+ -states are almost indistinguishable. It therefore comes as a surprise that their magneto-tunneling maps develop so differently. The reason for this striking fact is that not only the amplitude of the wave functions is relevant for the tunneling maps but also their phase. This is most easily seen when the slight elongation of the dot is neglected for the moment. For a circular dot in a magnetic field there are two p -states with opposite angular momentum $l^{QD} = -1$ and $l^{QD} = +1$, which have the same or the opposite sense of rotation as the emitter states, respectively. If we only take the angular part M_θ of the overlap integral in Eq. 3, and consider the emitter state with angular momentum $l = -1$, we find

$$M_\theta = \int_0^{2\pi} e^{-il^{QD}\theta} e^{-i\theta} d\theta = \begin{cases} 2\pi & \text{for } l^{QD} = -1 \\ 0 & \text{for } l^{QD} = +1 \end{cases}. \quad (5)$$

This explains why, at a high magnetic field of 9 T, the overlap of the p^+ level with the $l = -1$ emitter state is almost an order of magnitude smaller than with the p^- dot state. Therefore, the p^+ -state is mainly mapped out by the 'sharp tip' of the $l = 0$ emitter state, so that the map gives an accurate image of the wave function in momentum space. On the other hand, the magneto-tunneling map of the p^- -state is dominated by the contribution of the $l = -1$ 'annular tip' at high magnetic fields and this contribution is maximum when the wave functions are concentric (unshifted), i.e., for $B_x = B_y = 0$. This leads to the pronounced maximum in the center of the magneto-tunneling map found in both experiment and theory

at $B_z = 9$ T.

Our measurement thus clearly demonstrate that not only the amplitude of the wave function determines the tunneling characteristics but also the sign of the phase factor. It should be pointed out, though, that our experiment is only sensitive to the phase factor *relative to that of the back contact*. In this respect, the experimental situation is similar to optical holography, where also the phase sensitivity is made possible by comparison with a reference system.

I. METHODS

The investigated samples were grown by solid-source molecular beam epitaxy on a GaAs(100) semi-insulating substrate. The active part of the structure (see Fig. 1, left) starts with a 300 nm GaAs buffer, followed by a 20 nm thick Si-doped back contact and a 42.5 nm GaAs tunneling barrier. The dot layer was grown by depositing about 1.5 monolayers of InAs at 570° , leading to a dot density of about $1 \times 10^{10} \text{ cm}^{-2}$, and covered by 30 nm GaAs. The blocking layer consists of a 216 nm thick $\text{Al}_{0.75}\text{Ga}_{0.25}\text{As}$ digital alloy, capped by 10 nm GaAs. Ohmic contacts were provided by alloying AuGa pads and the gate electrode was prepared by evaporating NiCr and using standard optical lithography. All measurements were performed at 4.2 K in a liquid-He cryostat equipped with a superconducting solenoid and a 2-axes rotational sample holder. The capacitance-voltage traces were recorded at 6033 Hz using standard lock-in technique with $V_{mod} \approx 5$ mV.

-
- [1] D. R. Hofstadter, Phys. Rev. B **14**, 2239 (1976).
 - [2] for a review, see, e.g.: D. Bimberg, M. Grundmann, N. N. Ledentsov, *Quantum Dot Heterostructures*, Wiley, New York (1998).
 - [3] H. Drexler, D. Leonard, W. Hansen, J. P. Kotthaus and P. M. Petroff, Phys. Rev. Lett. **73**, 2252 (1994).
 - [4] M. Fricke, A. Lorke, J. P. Kotthaus, G. Medeiros-Ribeiro, and P. M. Petroff, Europhys. Lett. **36**, 197 (1996).
 - [5] E. E. Vdovin, A. Levin, A. Patane, *et al.*, Science **290**,122 (2000).
 - [6] R. J. Warburton *et al.*, Phys. Rev. B **58**, 16221 (1998).

- [7] D. Reuter, P. Kailuweit, A. D. Wieck, U. Zeitler, O. Wibbelhoff, C. Meier, A. Lorke, and J. C. Maan, *Phys. Rev. Lett.* **94**, 026808 (2005).
- [8] O. S. Wibbelhoff, A. Lorke, D. Reuter, and A. D. Wieck, *Appl. Phys. Lett.* **86**, 092104 (2005), *Appl. Phys. Lett.* **88**, 129901 (2006).
- [9] W. Lei, O. Wibbelhoff, C. Notthoff, B. Marquardt, D. Reuter, A.D. Wieck, A. Lorke, *Physica E* **40**, 1870 (2008).
- [10] A. Patane, *et al.*, *Phys. Rev. B* **65**, 165308 (2002).
- [11] R. J. Luyken, A. Lorke, A. O. Govorov, J. P. Kotthaus, G. Medeiros-Ribeiro and P. M. Petroff, *Appl. Phys. Lett.* **74**, 2486 (1999).
- [12] G. Bester *et al.*, *Phys. Rev. B* **76**, 075338 (2007).
- [13] Each state is split up into two because of the spin degree of freedom. Because of the low effective mass and the small g -factor in the present system, the influence of the external field on the spin can be neglected here.
- [14] G. Bester, A. Zunger, X. Wu, and D. Vanderbilt, *Phys. Rev. B* **74**, 081305(R) (2006).
- [15] Treating the back contact as two-dimensional has the advantage, that the influence of (B_x, B_y) on the states in the back contact does not need to be taken into account. This simplifies the calculation and makes the results easier to interpret. Experimentally, samples with two-dimensional and three dimensional back contacts show qualitatively similar results.
- [16] J. H. Davies, *The Physics of Low-Dimensional Semiconductors*, Cambridge University Press, Cambridge (1998).